

Strong Pinning Enhancement in MgB₂ Using Very Small Dy₂O₃ Additions

S. K. Chen, M. Wei and J. L. MacManus-Driscoll

Abstract

0.5 – 5.0 wt.% Dy₂O₃ was *in-situ* reacted with Mg + B to form pinned MgB₂. While T_c remained largely unchanged, J_c was strongly enhanced. The best sample (only 0.5 wt.% Dy₂O₃) had a $J_c \sim 6.5 \times 10^5 \text{ Acm}^{-2}$ at 6K, 1T and $3.5 \times 10^5 \text{ Acm}^{-2}$ at 20K, 1T, around a factor of 4 higher compared to the pure sample, and equivalent to hot-pressed or nano-Si added MgB₂ at $\leq 1\text{T}$. Even distributions of nano-scale precipitates of DyB₄ and MgO were observed within the grains. The room temperature resistivity decreased with Dy₂O₃ indicative of improved grain connectivity.

Applications in the temperature window of 20 – 26K are of particular interest for MgB₂. A near term goal is MRI coils operating at 2 – 4 T. To date, various mechanical processing methods¹⁻³ and nano-particle inclusions, in some cases with lattice doping (Y₂O₃⁴, nano-Si⁵ and SiC⁶ additions) have been demonstrated to increase the critical current density, J_c .

Trace amounts of oxygen during sample preparation can be both detrimental and beneficial to the current carrying properties of MgB₂. Oxide nano-phases have great potential to act as pinning centres but only if they are of the correct size and distribution, namely if they are incorporated within the grains and not at the grain boundaries. Formation of MgO and other Mg-B-O phases readily occurs depending on the processing conditions⁷⁻⁹. MgO has been shown to lead to isotropic pinning in films deposited in oxygen atmospheres¹⁰ but the adverse effect of excess oxide phases at grain boundaries results in a degradation of grain connectivity¹¹. Other structural defects which are effective pinning centres include dislocations¹² and grain boundaries¹³.

Previously, rather large additions (10 wt.%) of Y₂O₃ (which formed YB₄ and MgO nanoparticles when reacted with MgB₂) were found to increase both J_c and irreversibility field despite the fact that the samples were nearly insulating indicative of very poor connectivity⁴. The aim of this work is to study much lower levels of rare earth oxide additions in order to enhance intragrain pinning without degrading the grain boundaries. Dy₂O₃ was used instead of Y₂O₃ since Dy is the cheapest of all the rare earth elements. According to the phase diagram of Dy-B¹⁴, similar dysprosium boride phases as those in the Y-B system⁴ form across the composition range.

The starting powders were crystalline magnesium (99.8 %, 325 mesh) from Alfa Aesar, amorphous boron (95 – 97 %) from Fluka, and 1 – 3 μm sized Dy₂O₃

(99.99 %) from Reacton. 0.5 - 5.0 wt.% additions of Dy_2O_3 were studied. The powders were well mixed by grinding in a mortar for 60 min. Pellets of 5 mm diameter were uniaxially pressed, wrapped with Ta foil in the presence of excess Mg shavings and sintered at 900°C for 15 min. using heating and cooling rates of 15 °C/min. X-ray powder diffraction (XRD) patterns in the step-scanning mode θ - 2 θ with 0.05° increment were recorded using a Philips PW1050 diffractometer with a Cu-K_α radiation source. Microstructures were observed using field emission gun scanning electron microscopy (FEG-SEM). High resolution transmission electron microscopy (TEM) was undertaken on thinned samples using a JEOL 4000EX MK II microscope operating at 400 kV. Room temperature resistivity was carried out according to the standard four point method. Magnetisation versus temperature measurements were obtained using a commercial Quantum Design DC Magnetic Properties Measurement System (MPMS-XL). Magnetisation hysteresis loops were performed on bar shaped samples with the magnetic field applied parallel to the longest dimension of the sample. Magnetic critical current density was estimated based on the critical state model¹⁵.

Fig. 1 shows XRD patterns of MgB_2 with different amounts of Dy_2O_3 additions. MgB_2 is always the main phase observed. MgO was also observed in all the samples. DyB_4 and unreacted Dy_2O_3 were found in all the doped samples in increasing amounts with increasing Dy_2O_3 additions. Clearly, not all the Dy_2O_3 underwent complete reaction with B. Within the limit of calculation error, the a and c lattice parameters obtained from Rietveld refinements (see Table 1) did not change with Dy_2O_3 addition except for the 5 wt.% sample which showed a slight increase in c . The geometric density showed that the pellets were slightly more dense with Dy_2O_3

addition level (1.44 gcm^{-3} for the 5 wt.% doped sample compared to 1.16 gcm^{-3} for the pure one (Table 1)).

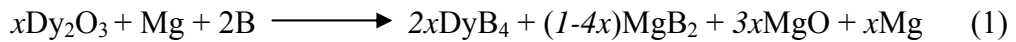
From the FEG-SEM images of the pure and 0.5 wt.% doped samples of Figs. 2a and 2b, a moderate refinement of grain morphology (100 – 200 nm cf. 500 nm) can be seen. However, in the pure samples (Fig. 2a), some fine particles of tens of nm size were also found among the bigger grains.

Fig. 2(c) shows a bright-field TEM image of a 0.5 wt.% Dy_2O_3 added sample. Nano-sized ($\sim 10\text{nm}$) precipitates of DyB_4 and MgO were observed inside the MgB_2 matrix. A low density of larger precipitates of the size of $\sim 70\text{nm}$ were also observed in other regions of the sample. In Fig. 2(c), some precipitates show the so-called ‘line of no contrast’ which is present for a particle with a spherical strain field when a single reflection is operating. The line of no contrast lies perpendicular to the direction of \mathbf{g} , as described by Ashby and Brown¹⁶. Qualitatively, the size and detailed contrast observed depends on the magnitude of the particle radius, constrained strain and the order of the reflection. An increase in any of these parameters leads to an increase in the size of the strain field. Fig 2(d) shows a high resolution image of an intragrain nano inclusion ($< 5\text{nm}$) which can be indexed as DyB_4 . Both the DyB_4 particles *and* associated strain fields can act as effective pinning centres, thus enhancing $J_c(H)$.

Fig. 3 shows the field dependence of the magnetic critical current density measured at 6K. J_c is increased with Dy_2O_3 additions especially in the low field region, and the best result is achieved for the 0.5 wt.% Dy_2O_3 additions. J_c was slightly degraded by further additions although it was still higher than the undoped sample. 0.25 wt.% Dy_2O_3 additions (data not shown) yielded very similar J_c ’s as for the 5 wt.% doped sample. As shown in Table 1, $J_c(1\text{T})$ at 6K and 20K of the 0.5 wt.%

sample was increased by a factor of more than 4 compared to the pure sample. As shown in the inset of Fig. 3 and in Table 1, T_c remains largely unchanged. However, the 5 wt.% Dy_2O_3 sample showed a slightly reduced T_c of 37.5K. We recall that the c parameter for the 5 wt.% Dy_2O_3 sample was also marginally higher. These two findings suggest that for the higher doping level there is either a very small level of Dy for Mg substitution, or a perturbation of the B planes by the nanoparticles.

As shown in Table 1, except for the 0.5 wt.% sample, the room temperature resistivity (ρ) was reduced with Dy_2O_3 additions. This trend was reproduced in a second batch of samples. ρ for the pure sample was higher than very clean bulk MgB_2 i.e. $62.2 \mu\Omega \text{ cm}$ compared to around $15 \mu\Omega \text{ cm}$ ¹⁷, However, for the 0.5 wt.% sample ρ was low compared to SiC doped samples, i.e. $75 \mu\Omega \text{ cm}$ compared to $522 \mu\Omega \text{ cm}$ ¹⁷. At first, the results are surprising since ρ would be expected to increase across the series as a result of increased impurity scattering. An explanation for this is proposed by the reaction equation (1):



Equation (1) shows the competing effects of (a) a decrease in ρ because of excess Mg which results because the B is reacted with some Dy and not all the Mg, and (b) an increase in ρ due to extra scattering from the DyB_4 , MgO and unreacted Dy_2O_3 . For every five moles of $(\text{DyB}_4 + \text{MgO})$ formed, there is one mole of Mg produced. The nanoparticles of DyB_4 and MgO were found to be largely incorporated *within* the grains. The fact that ρ shows a broadly decreasing trend suggests that the smaller amounts of evolved Mg were incorporated in the grain boundary regions. The amount

of unreacted Mg is sufficiently small so as not be detectable by X-ray diffraction. The presence of unreacted Mg in MgB₂ has previously been shown to reduce ρ greatly¹⁸.

Fig. 4 compares the field dependence of the magnetic J_c from this work to MgB₂ samples which have shown improved low-field J_c 's, namely hot isostatically pressed (HIPed), mechanically milled (nano-grain) material, either pure¹ or carbon doped²; HIPed pure (micro-grain) material⁵; and cold uniaxially pressed nano-Si⁵ and SiC doped⁶ samples. With the exception of the pure HIPed sample⁵, for all the literature samples in Fig. 4 the relative J_c enhancement from either pinning or doping is uncertain, i.e. samples containing Si, and/or C, and ball milled samples all show slightly reduced T_c 's indicative of doping, and this explains the good J_c performance at $> 2T$. It is the $< 1-2T$ regime that needs to be studied carefully to assess the influence of the pinning alone.

At 6K, 0-2T, the J_c for the 0.5 wt.% Dy₂O₃ added sample is slightly higher than the HIPed pure sample⁵. At self-field, J_c cannot be assessed accurately from magnetic data because of the flux jumping and also the sample is not fully field penetrated. However, at 20K and below 2T, the J_c of the Dy₂O₃ sample outperforms the ball milled nano-grain pure¹ and carbon doped² samples. It is similar to the pure HIP'ed⁵ and nano-Si doped⁵ samples at $\leq 1T$. The best sample from this work together with the 5 wt.% nano-Si doped⁵ sample likely represent the most highly pinned MgB₂ bulk material. By hiping such pinned materials, it should be possible to achieve J_c 's in excess of 1 MAcm⁻² at 20K, 2T. Alternately, through C doping of the pinned material, there is the possibility to achieve J_c 's of 10⁵ Acm⁻² at $\sim 4T$, 20K.

In summary, a very simple method of reacting very small amounts of Dy₂O₃ (~ 0.5 wt. %) with Mg and B to significantly increase pinning in MgB₂ has been demonstrated. T_c is preserved at around 38K. High resolution TEM imaging shows

nano-scale precipitates of DyB₄ and MgO within the grains. The surprising decrease in room temperature resistivity with Dy₂O₃ additions is believed to be due to unreacted Mg which decreases the intergrain resistivity.

We are grateful to EPSRC, UK for funding this work. S. K. Chen acknowledges UPM for the financial assistance.

- ¹ A. Gumbel, J. Eckert, G. Fuchs, K. Nenkov, K. H. Muller, and L. Schultz, Appl. Phys. Lett. **80** (2002) 2725.
- ² B. J. Senkowicz, J. E. Giencke, S. Patnaik, C. B. Eom, E. E. Hellstrom, and D. C. Larbalestier, Appl. Phys. Lett. **86** (2005) 202502.
- ³ N. A. Frederick, S. Li, M. B. Maple, V. F. Nesterenko, and S. S. Indrakanti, Physica C **363** (2001) 1.
- ⁴ J. Wang, Y. Bugoslavsky, A. Berenov, L. Cowey, A. D. Caplin, L. F. Cohen, J. L. MacManus-Driscoll, L. D. Cooley, X. Song, and D. C. Larbalestier, Appl. Phys. Lett. **81** (2002) 2026.
- ⁵ X. L. Wang, S. Soltanian, M. James, M. J. Qin, J. Horvat, Q. W. Yao, H. K. Liu, and S. X. Dou, Physica C **408-10** (2004) 63.
- ⁶ S. X. Dou, S. Soltanian, J. Horvat, X. L. Wang, S. H. Zhou, M. Ionescu, H. K. Liu, P. Munroe, and M. Tomsic, Appl. Phys. Lett. **81** (2002) 3419.
- ⁷ R. F. Klie, J. C. Idrobo, N. D. Browning, K. A. Regan, N. S. Rogado, and R. J. Cava, Appl. Phys. Lett. **79** (2001) 1837.
- ⁸ X. Z. Liao, A. C. Serquis, Y. T. Zhu, J. Y. Huang, D. E. Peterson, F. M. Mueller, and H. F. Xu, Appl. Phys. Lett. **80** (2002) 4398.

- ⁹ K. A. Yates, Z. Lockman, A. Kursumovic, G. Burnell, N. A. Stelmashenko, J. L. MacManus-Driscoll, and M. G. Blamire, *Appl. Phys. Lett.* **86** (2005) 022502.
- ¹⁰ M. Haruta, T. Fujiyoshi, T. Sueyoshi, K. Miyahara, T. Doi, H. Kitaguchi, S. Awaji, and K. Watanabe, *Supercond. Sci. Technol.* **18** (2005) 1460.
- ¹¹ P. Kovac, I. Hüge, T. Meligek, J. C. Grivel, W. Pachla, V. Strbik, R. Diduszko, J. Homeyer, and N. H. Andersen, *Supercond. Sci. Technol.* **17** (2004) L41.
- ¹² A. Serquis, X. Z. Liao, Y. T. Zhu, J. Y. Coulter, J. Y. Huang, J. O. Willis, D. E. Peterson, F. M. Mueller, N. O. Moreno, J. D. Thompson, V. F. Nesterenko, and S. S. Indrakanti, *J. Appl. Phys.* **92** (2002) 351.
- ¹³ H. Kitaguchi, A. Matsumoto, H. Kumakura, T. Doi, H. Yamamoto, K. Saitoh, H. Sotiati, and S. Hata, *Appl. Phys. Lett.* **85** (2004) 2842.
- ¹⁴ T. B. Massalski, *Binary Alloy Phase Diagrams*, 2nd ed. (ASM International, Materials Park, OH, 1990).
- ¹⁵ D. X. Chen and R. B. Goldfald, *J. Appl. Phys.* **66** (1989) 2489.
- ¹⁶ M. F. Ashby and L. M. Brown, *Phil. Mag.* **8** (1963) 1083.
- ¹⁷ S. X. Dou, V. Braccini, S. Soltanian, R. Klie, Y. Zhu, S. Li, X. L. Wang, and D. Larbalestier, *J. Appl. Phys.* **96** (2004) 7549.
- ¹⁸ C. U. Jung, H. J. Kim, M. S. Park, M. S. Kim, J. Y. Kim, Z. Du, S. I. Lee, K. H. Kim, J. B. Betts, M. Jaime, A. H. Lacerda, and G. S. Boebinger, *Physica C* **377** (2002) 21.

Table 1 Lattice constants, density, room temperature resistivity, T_c and J_c of the pure and Dy₂O₃ added samples.

Dy ₂ O ₃ addition (wt.%)	Lattice parameters		Density (gcm ⁻³)	ρ_{290K} ($\mu\Omega$ cm)	T_c (K)	J_c (Acm ⁻²)	
	$a(\text{\AA})$	$c(\text{\AA})$				6K, 1T	20K, 1T
0	3.0846(4)	3.5253(3)	1.16	62.2	38.0	1.5×10^5	8.0×10^4
0.5	3.0839(6)	3.5254(6)	1.27	75.0	38.0	6.5×10^5	3.5×10^5
1.0	3.0845(4)	3.5254(4)	1.27	46.5	38.0	4.9×10^5	2.5×10^5
2.0	3.0843(4)	3.5254(4)	1.32	42.6	38.0	5.0×10^5	2.3×10^5
5.0	3.084(1)	3.526(1)	1.44	24.0	37.5	4.2×10^5	2.2×10^5

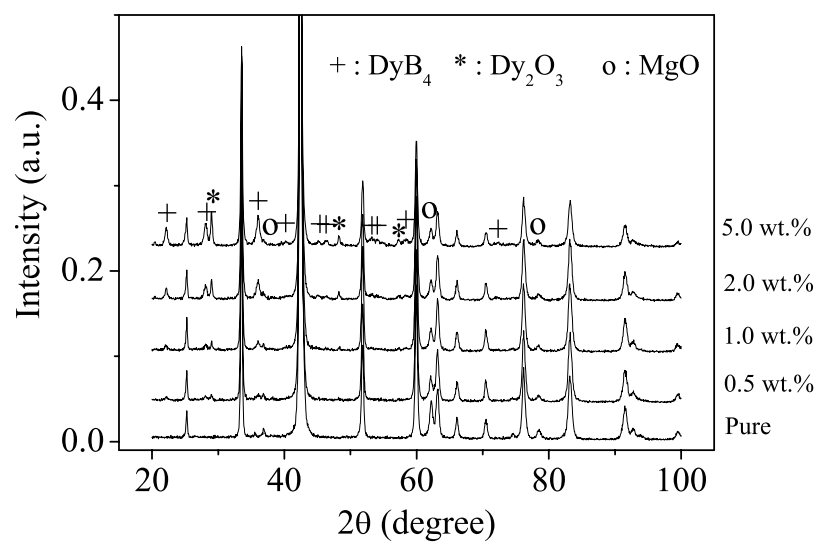


Fig. 1 X-ray diffraction patterns of the pure and Dy_2O_3 added samples.

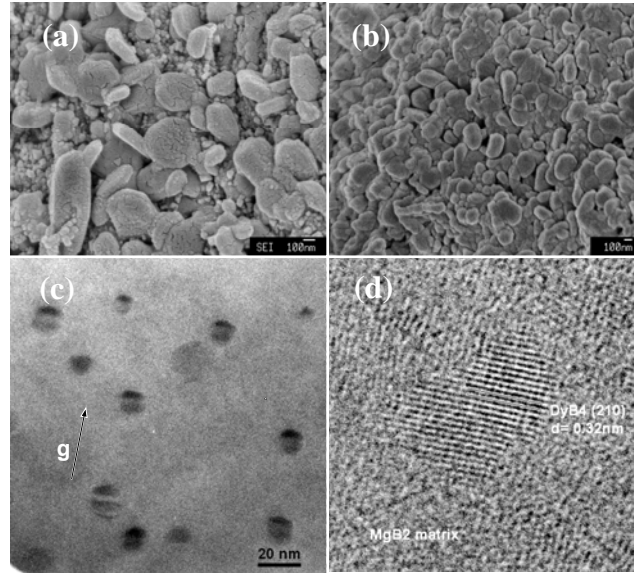


Fig. 2 FEG-SEM images of the (a) pure MgB₂ and (b) sample added with 0.5 wt.% of Dy₂O₃. (c) Bright-field TEM micrograph of MgB₂ matrix strain field contrast with a high order matrix reflection. The reciprocal lattice vector **g** is indicated by an arrow. (d) HRTEM image showing the (210) lattice fringe of a nano-sized DyB₄ precipitate.

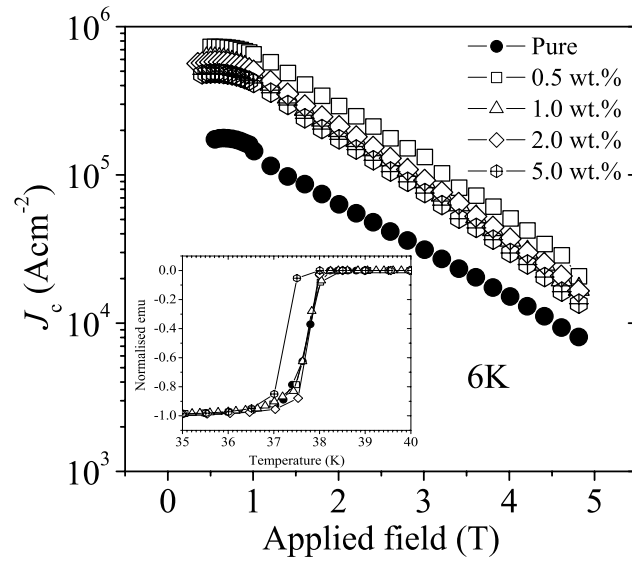


Fig. 3 Field dependence of magnetic J_c at 6K. Inset: Temperature dependence of normalised magnetic moment.

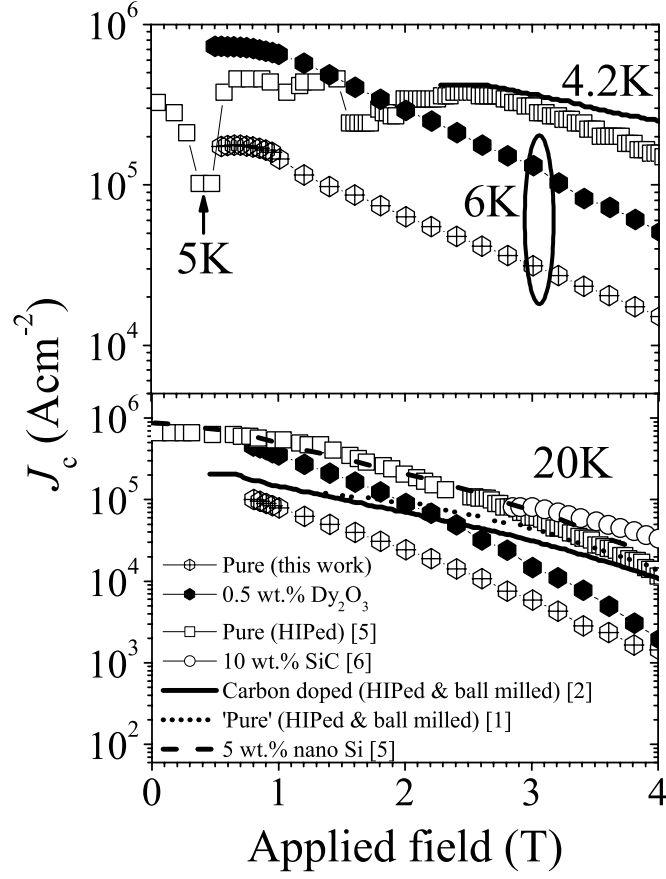


Fig. 4 J_c of the pure and best sample in comparison with those from references 1, 2, 5 and 6. Data on J_c below 6K are not available in some of the cited references.